



**HAL**  
open science

## Hydro-mechanical behaviour of high-density bentonite pellet on partial hydration

B Darde, A M Tang, Jean-Michel Pereira, J-N Roux, P Dangla, J Talandier,  
M N Vu

► **To cite this version:**

B Darde, A M Tang, Jean-Michel Pereira, J-N Roux, P Dangla, et al.. Hydro-mechanical behaviour of high-density bentonite pellet on partial hydration. *Géotechnique Letters*, 2018, 8 (4), pp.330 - 335. 10.1680/jgele.18.00114 . hal-04322973

**HAL Id: hal-04322973**

**<https://hal.science/hal-04322973v1>**

Submitted on 10 Jan 2024

**HAL** is a multi-disciplinary open access archive for the deposit and dissemination of scientific research documents, whether they are published or not. The documents may come from teaching and research institutions in France or abroad, or from public or private research centers.

L'archive ouverte pluridisciplinaire **HAL**, est destinée au dépôt et à la diffusion de documents scientifiques de niveau recherche, publiés ou non, émanant des établissements d'enseignement et de recherche français ou étrangers, des laboratoires publics ou privés.

- Date text written: October 24, 2018
  - 1991 words in the main text
  - 2 Tables
  - 9 Figures
- 

## **Hydro-mechanical behaviour of high-density bentonite pellet upon partial hydration**

### Author 1

- DARDE Benjamin
- Affiliation:
  - Université Paris-Est, Laboratoire Navier, UMR 8205 (Ecole des Ponts ParisTech – Ifsttar – CNRS), Marne-la-Vallée, France
  - French National Radioactive Waste Management Agency (Andra), Châtenay-Malabry, France

### Author 2

- TANG Anh Minh
- Affiliation:
  - Université Paris-Est, Laboratoire Navier, UMR 8205 (Ecole des Ponts ParisTech – Ifsttar – CNRS), Marne-la-Vallée, France

### Author 3

- PEREIRA Jean-Michel
- Affiliation:
  - Université Paris-Est, Laboratoire Navier, UMR 8205 (Ecole des Ponts ParisTech – Ifsttar – CNRS), Marne-la-Vallée, France

### Author 4

- ROUX Jean-Noël
- Affiliation:
  - Université Paris-Est, Laboratoire Navier, UMR 8205 (Ecole des Ponts ParisTech – Ifsttar – CNRS), Marne-la-Vallée, France

### Author 5

- DANGLA Patrick
- Affiliation:
  - Université Paris-Est, Laboratoire Navier, UMR 8205 (Ecole des Ponts ParisTech – Ifsttar – CNRS), Marne-la-Vallée, France

### Author 6

- TALANDIER Jean
- Affiliation:
  - French National Radioactive Waste Management Agency (Andra), Châtenay-Malabry, France

### Author 7

- VU Minh Ngoc
- Affiliation:
  - French National Radioactive Waste Management Agency (Andra), Châtenay-Malabry, France

### **Corresponding author:**

**Dr. Anh Minh TANG**  
**Ecole des Ponts ParisTech**  
**Laboratoire Navier/Géotechnique (CERMES)**  
**6-8 avenue Blaise Pascal**  
**77455 MARNE-LA-VALLÉE**  
**France**  
**Email: anh-minh.tang@enpc.fr**

### **Abstract (150 words)**

The hydro-mechanical behaviour of a high-density bentonite pellet, potential candidate for engineered barriers in high-level radioactive waste disposal, is investigated through laboratory tests. Water content and volumetric strain are first determined at various suctions (ranging from 9 MPa to 89 MPa) during partial hydration from its initial state. Afterward, compression tests allow the Young modulus and strength to be determined at various suctions. The experimental results are then interpreted by using an existing model describing the hydro-mechanical behaviour of an aggregate in compacted expansive clay. The analyses show that a single set of parameters is sufficient to predict the suction dependency of volumetric strain, Young modulus and compressive strengths. These findings would be helpful for further numerical investigations on the hydro-mechanical behaviour of granular bentonite-based engineered barriers by using both finite element and discrete element methods.

**Keywords:** Partial saturation; Expansive soils; Laboratory tests.

### **List of notations**

$\rho_s$ : particle density

$\rho_d$ : dry density

$e$ : void ratio

$w$ : water content

$D$ : pellet's diameter

$H$ : pellet's total height

$h$ : pellet's cylinder-shaped part height

$R_c$ : pellet's curvature radius

$s_0$ : initial suction

$\varepsilon_a$ : axial strain

$\varepsilon_r$ : radial strain

$\varepsilon_v$ : volumetric strain

$N$ : axial load

$E$ : Young modulus

$\nu$ : Poisson ratio

$\delta_n$ : normal displacement

$S_r$ : degree of saturation

$R_R$ : normal force at failure during radial compression

$R_A$ : normal force at failure during axial compression

$K_m$ : microstructural bulk modulus

$\hat{p}$ : effective mean stress

$\alpha_m$ : material parameter

$\beta_m$ : material parameter

$C_A$ : material parameter relating axial strength to modulus

$C_R$ : material parameter relating radial strength to modulus

1 **Introduction**

2 Bentonite-based materials are considered as candidate materials for engineered barriers in  
3 radioactive waste disposal due to their low permeability, good radionuclides retention capacity,  
4 and ability to swell upon hydration, which is an important property to fill the technological voids.  
5 While many studies on the hydro-mechanical behaviour of bentonite-based engineered barriers  
6 have focused on compacted blocks of bentonite, bentonite pellets/powder mixtures have also  
7 been considered as an interesting alternative (Volckaert et al., 1996; van Geet et al., 2005;  
8 Imbert and Villar, 2006; Hoffman et al., 2007; Alonso et al., 2011; Gens et al., 2011; Molinero-  
9 Guerra et al., 2017).

10

11 After Kröhn (2005), vapour diffusion plays a significant – if not dominant – role in the  
12 resaturation process of bentonite-based engineered barriers. In order to study the hydro-  
13 mechanical behaviour of bentonite pellets mixtures upon hydration by vapour transfer,  
14 accounting for the granular nature of the material (Molinera-Guerra et al., 2018*a,b*), numerical  
15 simulations based on the discrete element method (DEM) (Cundall and Strack, 1979; Roux and  
16 Chevoir, 2005; Agnolin and Roux, 2007; Than et al., 2017) could be an interesting way of  
17 assessing the influence of pellets swelling on the mixtures behaviour. In DEM simulations, each  
18 particle is modelled individually. A model describing the hydro-mechanical behaviour of a single  
19 pellet is therefore required. As this approach is valid for granular materials, the model has to  
20 focus on hydration state at which a pellet has not lost its initial structure.

21

22 For this purpose, the present study focuses on the hydro-mechanical behaviour of a single  
23 pellet upon partial hydration. The vapour equilibrium technique is used to hydrate the pellet. At  
24 equilibrium, the pellet volume and water content are determined, which allows determining the  
25 relationship between volumetric strain and suction. Afterward, a compression test is performed  
26 on the pellet to determine its stiffness and strength. Finally, the results are interpreted through  
27 the conceptual framework proposed by Alonso et al. (1999).

28

29 **2. Material**

30 The material characterised in this study are sub-spherical MX80 bentonite pellets. MX80 is a  
31 Na-bentonite from Wyoming, with high smectite contents, which main physical properties are  
32 summarised in Table 1. Pellets are obtained through compaction of bentonite powder. They are  
33 composed of a cylinder-shaped part and two spherical ends (Figure 1). Their initial properties  
34 are shown in Table 2.

35

### 36 **3. Experimental methods**

37 Suction-controlled hydration is performed through the vapour equilibrium technique (Tang and  
38 Cui, 2005; Delage et al., 2006). Pellets are placed within a desiccator containing a saturated salt  
39 solution. When equilibrium is reached (verified by pellet mass), the pellets dimensions are  
40 measured using a camera (one picture is taken from the side, Figure 1a, and pellet's height and  
41 diameter are measured with an accuracy of 0.01 mm). Axial strain  $\varepsilon_a$  and radial strain  $\varepsilon_r$  are  
42 determined by comparison of height and diameter with their initial values. Volumetric strain  $\varepsilon_V$  is  
43 calculated as follows:

$$\varepsilon_V = (1 + \varepsilon_a)(1 + \varepsilon_r)^2 - 1 \quad (1)$$

44 Compression tests are carried out by using a load frame (Figure 2). The displacement rate is  
45 imposed at 0.1 mm/min. Displacements are recorded by a displacement transducer and the  
46 contact force between the pellet and the frame is recorded by a force transducer (with an  
47 accuracy of 0.1 N).

48

49 Compression tests are performed in both axial and radial directions (Figure 3). In axial  
50 compression tests (Figure 3a), contact between the load frame and the pellet is sub-punctual.  
51 Assuming isotropic linear elastic behaviour, the Hertz law is adapted to obtain Young modulus  
52 (Johnson, 1985):

$$N = \frac{1}{3} \frac{E}{1 - \nu^2} (2R_c)^{1/2} \delta_n^{3/2} \quad (2)$$

53 Where  $N$  is the axial load;  $E$  and  $\nu$  are Young modulus and Poisson's ratio, respectively;  $\delta_n$  is  
54 the normal displacement.

55

56 In radial compression test (Figure 3b), the contact is assumed to be linear. Johnson (1985)'s  
 57 elasticity law, relating normal displacement to normal force for a contact between an infinite  
 58 plate and a cylinder, is applied to determine  $E$ .

$$\delta_n = 2 \frac{N}{h} \frac{1 - \nu^2}{\pi E} \left[ 2 \ln \left( 2 \sqrt{\frac{\pi D}{2} \frac{E}{1 - \nu^2} \frac{N}{h}} \right) - 1 \right] \quad (3)$$

59 Figure 4 presents the results corresponding to  $s = 89$  MPa. Several tests are performed and  
 60 one curve is chosen to show the method for determination of  $E$ . For axial compression tests  
 61 (Figure 4a),  $N$  increases with increasing displacement until failure. At failure,  $N$  decreases  
 62 abruptly. The Hertz law (equation 2) is then used to fit experimental data from the start to the  
 63 failure to determine  $E$ . In the present work,  $\nu = 0.3$  for the sake of simplicity. For radial  
 64 compression tests (Figure 4b),  $N$  increases with increasing displacement in two distinct phases:  
 65 first, a slow increase; second, a more significant and sub-linear increase. The first phase is  
 66 interpreted as the consequence of an imperfect contact between the frame and the pellet at the  
 67 beginning of the test. As displacement increases, the contact becomes linear and the force-  
 68 displacement relationship is significantly modified. Considering this hypothesis, equation (3) is  
 69 used to fit experimental data only from the start of the second phase to the failure.

70

71 In the present work, beside the initial suction, eight suctions (ranging from 9 MPa to 82 MPa)  
 72 are considered. For each one, several pellets are analysed to assess the repeatability of the  
 73 experimental data.

74

#### 75 **4. Experimental results**

76 Figure 5 presents  $w$  versus elapsed time during the suction equilibrium phase. From its initial  
 77 value (12.2%),  $w$  increases quickly during the first days and equilibrium is reached after 10  
 78 days, except for the lowest suction (9 MPa) where 30 days were necessary. The values  
 79 obtained at equilibrium (Figure 5) are then plotted versus imposed suction in Figure 6a. Along  
 80 the hydration path (decrease of suction from 89 MPa to 9 MPa)  $w$  increases from 12.2 % to 24.3  
 81 %. Results obtained on the same materials (MX80) in other studies are also plotted. Within the  
 82 investigated suction range,  $w$  -  $s$  relationships are similar and do not depend on the initial dry

83 density or hydration conditions. Figure 6b presents the degree of saturation ( $S_r$ ) versus suction  
84 which shows that  $S_r$  does not change significantly during this hydration phase.

85

86 Figure 7 presents the strains versus suction during this hydration phase.  $\epsilon_a$  is generally higher  
87 than  $\epsilon_r$ . The mean values of  $\epsilon_v$ , obtained from the mean values of  $\epsilon_a$  and  $\epsilon_r$ , are plotted. As  
88 expected,  $\epsilon_v$  keeps increasing upon hydration.

89

90 The mechanical properties ( $E$  and strength) are plotted versus suction in Figure 8. Moduli  
91 obtained for both axial and radial compression tests are similar (Figure 8a) and a single mean  
92 value is retained for both compression directions. These results confirm that the assumptions  
93 used to interpret the compression tests (isotropic linear elastic behaviour, equations 2 & 3) are  
94 appropriate. Upon hydration, the pellet modulus and strength decrease significantly.

95

96 Finally, the relationship between compressive strengths and modulus is presented in Figure 9. A  
97 linear relationship is suggested for both axial and radial directions.

98

## 99 **5. Model**

100 In the present work, the pellet initial dry density is high and its behaviour is assumed to be  
101 similar to that of an aggregate (*i.e.* the microstructural level) in compacted expansive clay  
102 following the model proposed by Alonso et al. (1999).

103 Microstructural volumetric strain is written:

$$d\epsilon_{vm} = \frac{d\hat{p}}{K_m} = \frac{ds}{K_m} \quad (4)$$

104

$$K_m(s) = \frac{1}{\beta_m} \exp(\alpha_m s) \quad (5)$$

105 Where  $K_m$  is the microstructural bulk modulus,  $\hat{p}$  is the effective mean stress (equal to  $s$  in the  
106 present study),  $\alpha_m$  and  $\beta_m$  are material parameters.

107

108 From compression tests results,  $\alpha_m = 0.024 \text{ MPa}^{-1}$  and  $\beta_m = 0.016 \text{ MPa}^{-1}$  are obtained through  
109 basic exponential regression (Figure 8a).



110

111 Integrating (5) from initial suction  $s_0$  to a given suction  $s$  leads to:

$$\varepsilon_{vm} = \frac{\beta_m}{\alpha_m} [\exp(-\alpha_m s_0) - \exp(-\alpha_m s)] \quad (6)$$

112 Where  $\alpha_m$  and  $\beta_m$  values, determined from compression tests results, are found to satisfactorily  
113 model the volumetric strain upon hydration (Figure 7).

114

115 From Figure 9, it seems convenient to propose a linear relationship between pellet strengths  
116 and modulus. The following relationships are proposed:

$$R_A = C_A E \quad (7)$$

117

$$R_R = C_R E \quad (8)$$

118 where  $C_A$  and  $C_R$  are material parameters relating the strength to the modulus for axial and  
119 radial compression tests, respectively.  $C_A = 1.206 \times 10^{-7} \text{ m}^{-2}$  and  $C_R = 1.816 \times 10^{-7} \text{ m}^{-2}$  following  
120 the fitting (Figure 9).

121

122 From (5), (7) and (8), the evolution of pellet strength upon hydration can be written:

$$R_A = 3 (1 - 2\nu) C_A \frac{1}{\beta_m} \exp(\alpha_m s) \quad (9)$$

123

$$R_R = 3 (1 - 2\nu) C_R \frac{1}{\beta_m} \exp(\alpha_m s) \quad (10)$$

124 Model predictions are presented in dash lines in Figure 9, along experimental results for  
125 comparison.

126

## 127 **6. Discussion**

128 The experimental results show that partial hydration induces an increase in water content and  
129 pellet volume and a decrease in Young modulus and strength. These trends agree with existing  
130 results on bentonite-based materials (Wiebe et al., 1998; Blatz et al., 2002; Lloret et al., 2003;  
131 Tang and Cui, 2009; Carrier et al., 2016). However, the volumetric strain obtained in the present  
132 work (50% for hydration from 89 MPa to 9 MPa) is higher than that observed on a single MX80

133 bentonite aggregate (25%, after Tang and Cui 2009). In addition, the Young modulus measured  
134 in the present work is generally one order of magnitude smaller than that measured by Carrier  
135 et al. (2016) on MX80 bentonite clay film over the same suction range. It means that the  
136 mechanical behaviour of the material is strongly dependent on the dimensions of the specimen.

137

138 In addition, it is interesting to note that the results obtained by compression tests (Figure 8a)  
139 can be used to predict the results obtained by hydration (Figure 7). The role of total stress is  
140 thus similar to that of suction as suggested by Alonso et al. (1999) for microstructural level.

141

142 The present work contributes to a more comprehensive approach to model the behaviour of a  
143 single pellet. These results would be helpful for further numerical investigations on the hydro-  
144 mechanical behaviour of granular bentonite using the finite element method with double-porosity  
145 models (i.e. Alonso et al., 2011) where a single pellet corresponds to the micro-structural level.  
146 Actually, Molinero Guerra et al. (2017) performed mercury intrusion porosimetry on a similar  
147 bentonite pellet and found that the volume of macro-pores is negligible at high suction. Besides,  
148 for numerical investigations using discrete element modelling, these results can be directly used  
149 to describe the behaviour of a single pellet under hydro-mechanical loading.

150

151 However, it is worthy to mention that the behaviour of the pellet observed in the present work  
152 doesn't correspond to all the assumptions proposed for an aggregate in the model of Alonso et  
153 al. (1999): (i) the pellet is not fully-saturated; (ii) its behaviour is not reversible; (iii) the volumetric  
154 behaviour of the pellet is not isotropic. In spite of these disagreements, the model would  
155 correctly predict the hydro-mechanical behaviour of a pellet during this partial hydration path (up  
156 to 9 MPa of suction). At suction lower than this value, the model would no longer be valid as the  
157 pellet would disaggregate (as suggested by Saiyouri et al. 2004 for bentonite particles, Koliji et  
158 al., 2010 and Cardoso et al., 2013 for clay aggregates less reactive than bentonite).

159

160 In addition to the volumetric behaviour, the strengths of the pellet under compression can be  
161 also predicted by using the same values of  $\alpha_m$  and  $\beta_m$ . These results can be explained by the  
162 linear correlation between the strengths and the modulus. Actually, correlations between these

163 two properties were observed on various compacted clayey soils (Lee et al., 2005; Zeh and  
164 Witt, 2007).

165

## 166 **7. Conclusions**

167 The behaviour of a single high-density bentonite pellet under hydration from 82 to 9 MPa of  
168 suction and the variation of its mechanical properties during this path are investigated in this  
169 study by laboratory tests. The results show an increase of pellet's volume and water content  
170 upon suction decrease. At the same time, its mechanical properties (Young modulus and  
171 strengths) decrease during hydration. When analysing the experimental result with an existing  
172 model for compacted expansive soil and assuming that the pellet behaviour is similar to that of  
173 an aggregate, a single set of parameters ( $\alpha_m$  and  $\beta_m$ ) can be used to predict the suction  
174 dependency of volumetric strain, Young modulus and strengths.

175

176 The results from this work would be helpful for further numerical investigations (finite element  
177 and discrete element methods) on the hydro-mechanical behaviour of granular bentonite-based  
178 engineered barrier for geological radioactive waste disposal during the first years following the  
179 installation.

180

## 181 **References**

182 Agnolin, I., & Roux, J. N. (2007). Internal states of model isotropic granular packings. I.

183 Assembling process, geometry, and contact networks. *Physical Review E - Statistical,*

184 *Nonlinear, and Soft Matter Physics*, 76(6), 1–27. <https://doi.org/10.1103/PhysRevE.76.061302>

185 Alonso, E. E., Vaunat, J., & Gens, A. (1999). Modelling the mechanical behaviour of

186 expansive clays. *Engineering Geology*, 54(1–2), 173–183. <https://doi.org/10.1016/S0013->

187 7952(99)00079-4

188 Alonso, E. E., Romero, E., & Hoffmann, C. (2011). Hydromechanical behaviour of

189 compacted granular expansive mixtures: experimental and constitutive study. *Géotechnique*,

190 61(4), 329–344. <https://doi.org/10.1680/geot.2011.61.4.329>

191 Blatz, J. A., Graham, J., & Chandler, N. A. (2002). Influence of suction on the strength  
192 and stiffness of compacted sand-bentonite. *Canadian Geotechnical Journal*, 39(5), 1005–1015.  
193 <https://doi.org/10.1139/t02-056>

194 Cardoso, R., Alonso, E.E, and Maranha das Neves, E. (2013) A constitutive model for  
195 compacted expansive and bonded marls. *Géotechnique*, 63(13), 1116 – 1130.  
196 <https://doi.org/10.1680/geot.12.P.101>

197 Cundall, P., & Strack, O. (1979). A discrete numerical model for granular assemblies.  
198 *Géotechnique*, 29(1), 47–65.

199 Delage, P., Marcial, D., Ruiz, X., & Cui, Y. J. (2006). Ageing effects in a compacted  
200 bentonite: a microstructure approach. *Géotechnique*, 56(5), 291–304.  
201 <https://doi.org/10.1680/geot.2006.56.5.291>

202 Gens, A., Valleján, B., Sánchez, M., Imbert, C., Villar, M. V., & Van Geet, M. (2011).  
203 Hydromechanical behaviour of a heterogeneous compacted soil: experimental observations and  
204 modelling. *Géotechnique*, 61(5), 367–386. <https://doi.org/10.1680/geot.SIP11.P.015>

205 Hoffmann, C., Alonso, E. E., & Romero, E. (2007). Hydro-mechanical behaviour of  
206 bentonite pellet mixtures. *Physics and Chemistry of the Earth*, 32(8–14), 832–849.  
207 <https://doi.org/10.1016/j.pce.2006.04.037>

208 Imbert, C., & Villar, M. V. (2006). Hydro-mechanical response of a bentonite  
209 pellets/powder mixture upon infiltration. *Applied Clay Science*, 32(3–4), 197–209.  
210 <https://doi.org/10.1016/j.clay.2006.01.005>

211 Johnson, K. L. (1985). *Contact Mechanics*. Cambridge, UK: Cambridge University  
212 Press. <https://doi.org/10.1115/1.3261297>

213 Koliji, A., Laloui, L. and Vulliet, L. (2010), Constitutive modeling of unsaturated  
214 aggregated soils. *Int. J. Numer. Anal. Meth.*, 34, 1846 – 1876. <https://doi.org/10.1002/nag.888>

215 Kröhn, K. P. (2005). New evidence for the dominance of vapour diffusion during the re-  
216 saturation of compacted bentonite. *Engineering Geology*, 82(2), 127–132.  
217 <https://doi.org/10.1016/j.enggeo.2005.09.015>

218 Lee, F. H., Lee, Y., Chew, S.-H., & Yong, K. Y. (2005). Strength and modulus of marine  
219 clay-cement mixes. *Journal of Geotechnical and Geoenvironmental Engineering*, 131(2), 178–  
220 186. [https://doi.org/10.1061/\(ASCE\)1090-0241\(2005\)131:2\(178\)](https://doi.org/10.1061/(ASCE)1090-0241(2005)131:2(178))

221 Lloret, A., Villar, M. V, Sanchez, M., Gens, A., Pintado, X., & Alonso, E. (2003).  
222 Mechanical behaviour of heavily compacted bentonite under high suction changes.  
223 *Geotechnique*, 53(1), 27–40. <https://doi.org/10.1680/geot.53.1.27.37258>

224 Molinero Guerra, A., Mokni, N., Delage, P., Cui, Y. J., Tang, A. M., Aïmedieu, P.,  
225 Bornert, M. (2017). In-depth characterisation of a mixture composed of powder/pellets MX80  
226 bentonite. *Applied Clay Science*, 135, 538–546. <https://doi.org/10.1016/j.clay.2016.10.030>

227 Molinero-Guerra, A., Aïmedieu, P., Bornert, M, Cui, Y.J., Tang, A.M., Sun, Z., Mokni, N.,  
228 Delage, P., Bernier, F. (2018a). Analysis of the structural changes of a pellet/powder bentonite  
229 mixture upon wetting by X-ray computed microtomography. *Applied Clay Science*. (doi:  
230 10.1016/j.clay.2018.07.043)

231 Molinero-Guerra, A., Cui, Y.J., Mokni, N., Delage, P., Bornert, M., Aïmedieu, P., Tang,  
232 A.M., & Bernier, F. (2018b). Investigation of the hydro-mechanical behaviour of a pellet/powder  
233 MX80 bentonite mixture using an infiltration column. *Engineering Geology*, 243, 18 – 25.

234 Roux, J.-N., & Chevoir, F. (2005). Généralités sur la simulation numérique discrète des  
235 matériaux granulaires, 254, 109–138.

236 Saiyouri, N., Tessier, D., & Hicher, P. Y. (2004). Experimental study of swelling in  
237 unsaturated compacted clays. *Clay Minerals*, 39(4), 469–479.  
238 <https://doi.org/10.1180/0009855043940148>

239 Tang, A.-M., & Cui, Y.-J. (2005). Controlling suction by the vapour equilibrium technique  
240 at different temperatures and its application in determining the water retention properties of  
241 MX80 clay. *Canadian Geotechnical Journal*, 42(1), 287–296. <https://doi.org/10.1139/t04-082>

242 Tang, A.M., Cui, Y.J. (2009). Modelling the thermo-mechanical behaviour of compacted  
243 expansive clays. *Géotechnique*, 59 (3), 185-195. (doi: 10.1680/geot.2009.59.3.185)

244 Than, V.D., Khamseh, S., Tang, A.M., Pereira, J.M., Chevoir, F., & Roux, J.N. (2017).  
245 Basic Mechanical Properties of Wet Granular Materials: A DEM Study. *J. Eng. Mech.*, 143(1),  
246 C4016001. (doi:10.1061/(ASCE)EM.1943-7889.0001043).

247 Van Geet, M., Volckaert, G., & Roels, S. (2005). The use of microfocus X-ray computed  
248 tomography in characterising the hydration of a clay pellet/powder mixture. *Applied Clay*  
249 *Science*, 29(2), 73–87. <https://doi.org/10.1016/j.clay.2004.12.007>

250 Volckaert, G., Bernier, F., Alonso, E. E., Gens, A., Samper, J., Villar, M. V., Martin-  
251 Martin, P. L., Cuevas, J., Campos, R., Thomas, H., Imbert, C. & Zingarelli, V. (1996). Thermal-  
252 hydraulic-mechanical and geochemical behaviour of the clay barrier in radioactive waste  
253 repositories (model development and validation), EUR 16744 EN. Luxembourg: Publications of  
254 the European Communities.

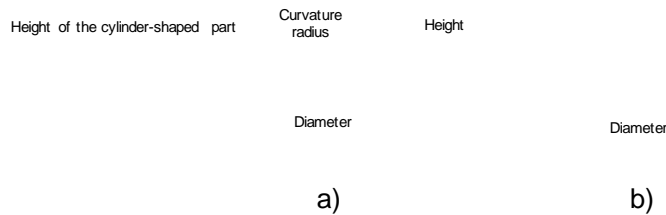
255 Wiebe, B., Graham, J., Tang, G. X., & Dixon, D. (1998). Influence of pressure,  
256 saturation, and temperature on the behaviour of unsaturated sand-bentonite. Canadian  
257 Geotechnical Journal, 35, 194–205. <https://doi.org/10.1139/t97-093>

258 Zeh, R. M., & Witt, K. J. (2007). The tensile strength of compacted clays as affected by  
259 suction and soil structure. Experimental Unsaturated Soil Mechanics, 112, 219–226.  
260 [https://doi.org/10.1007/3-540-69873-6\\_21](https://doi.org/10.1007/3-540-69873-6_21)

261

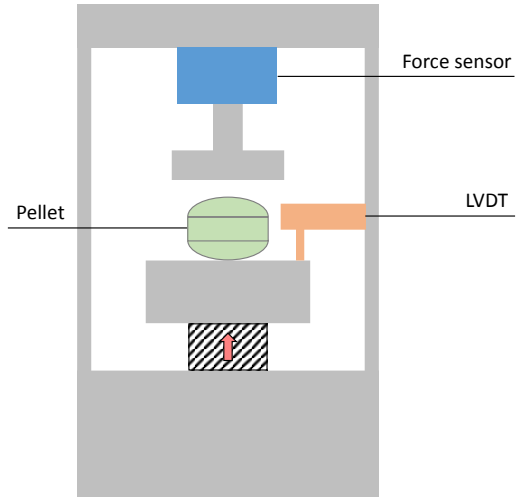
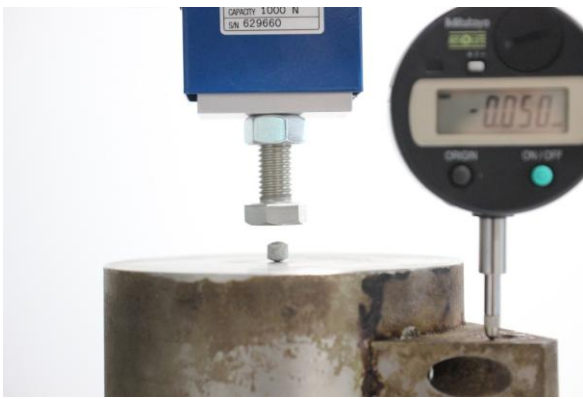
262 **Figure captions (images as individual files separate to your MS Word text file).**

263 Figure 1. Schematic views of a single pellet. Radial view (a) and axial view (b).



264

265 Figure 2. Load frame used to perform compression test. (a) Picture; (b) description



a)

b)

266

267

268

Figure 3. Schematic view of the compression tests: (a) axial compression; (b) radial compression.

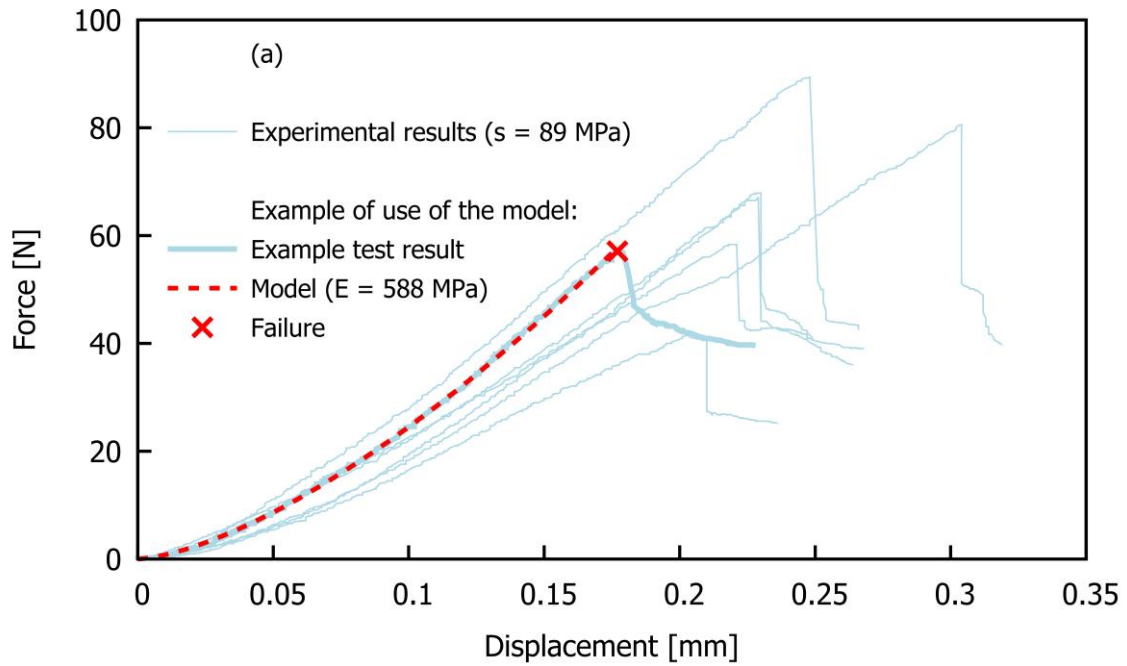
a)

b)

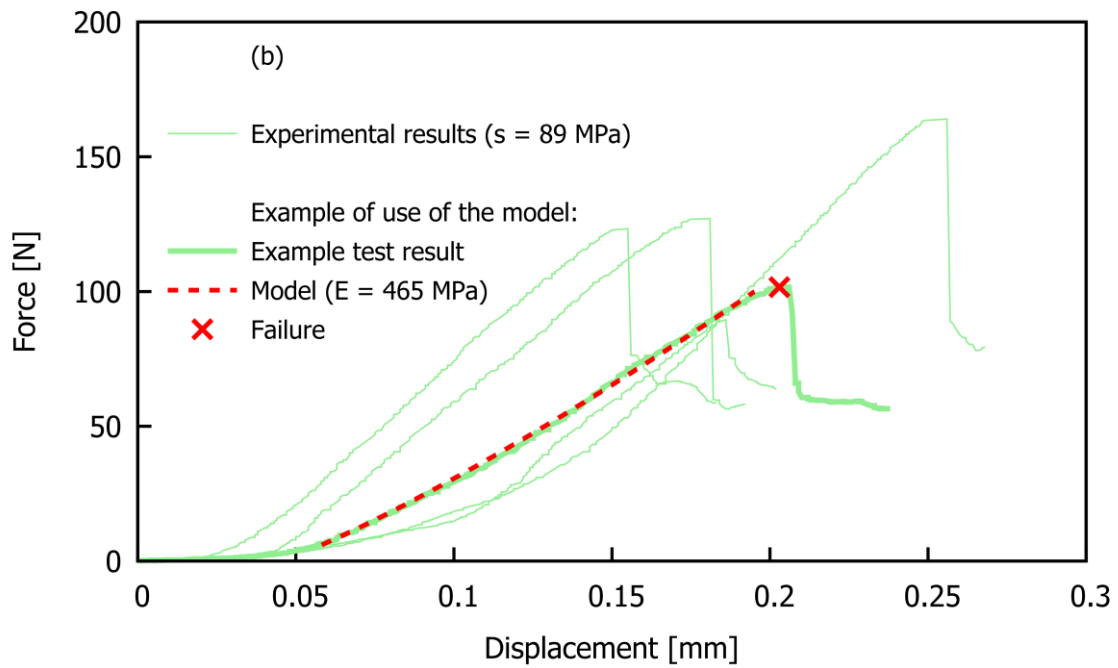
269

270

Figure 4. Typical results of compression tests: (a) axial compression; (b) radial compression.



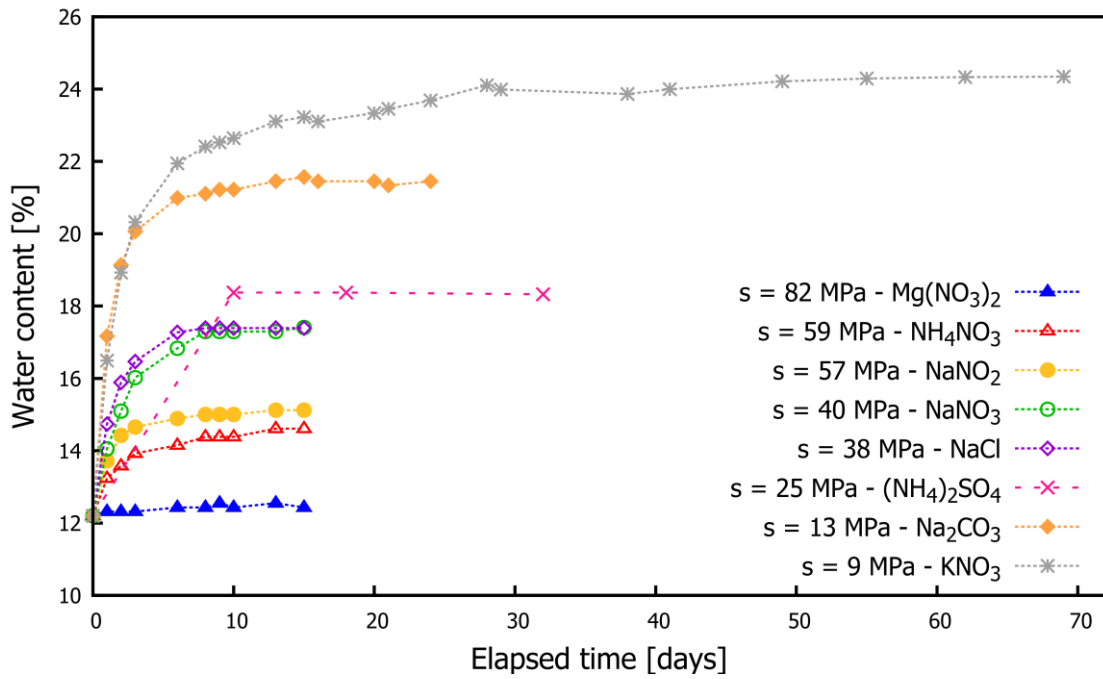
271



272

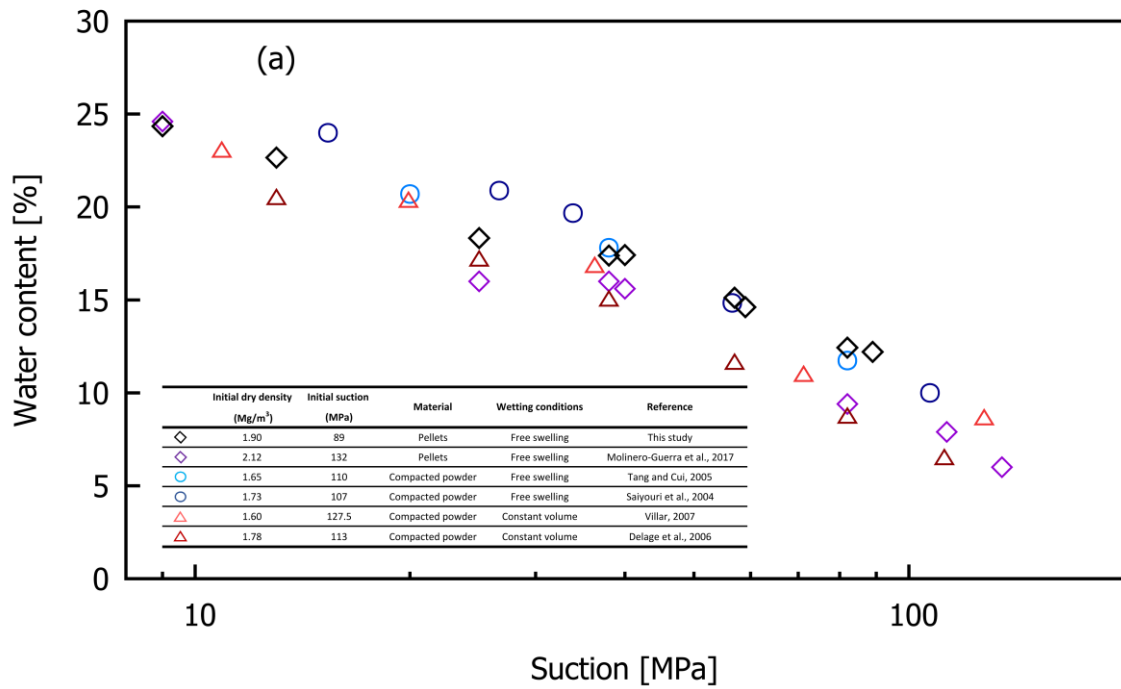
273 Figure 5. Water content versus elapsed time during the suction equilibrium phase.



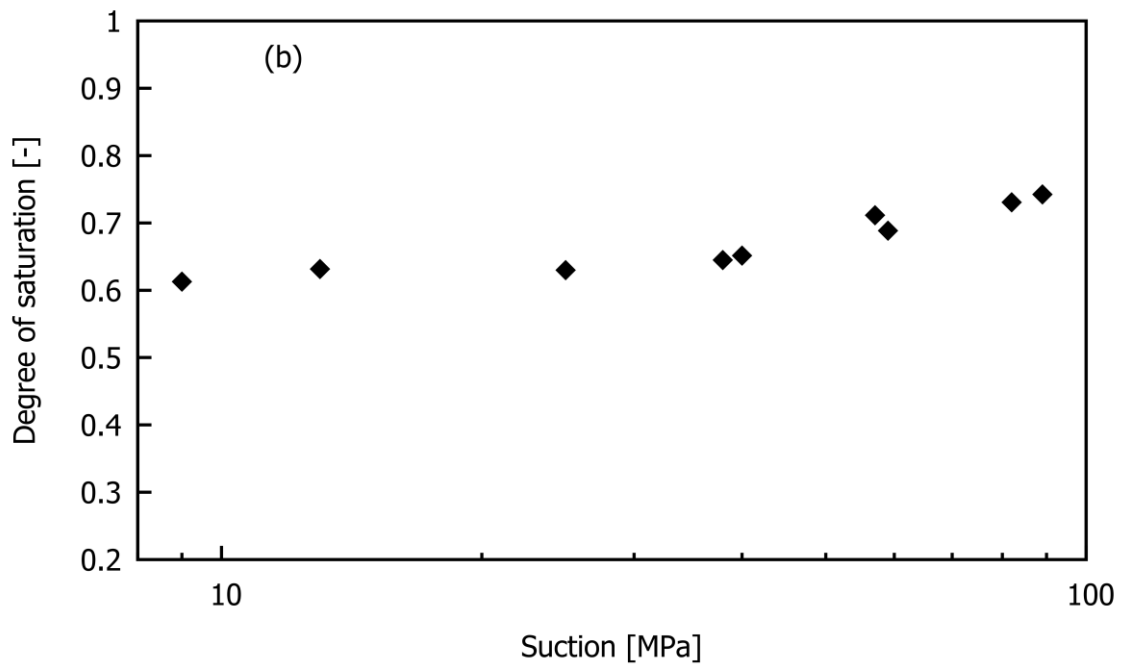


274

275 Figure 6. (a) Water content versus suction; (b) Degree of saturation versus suction.

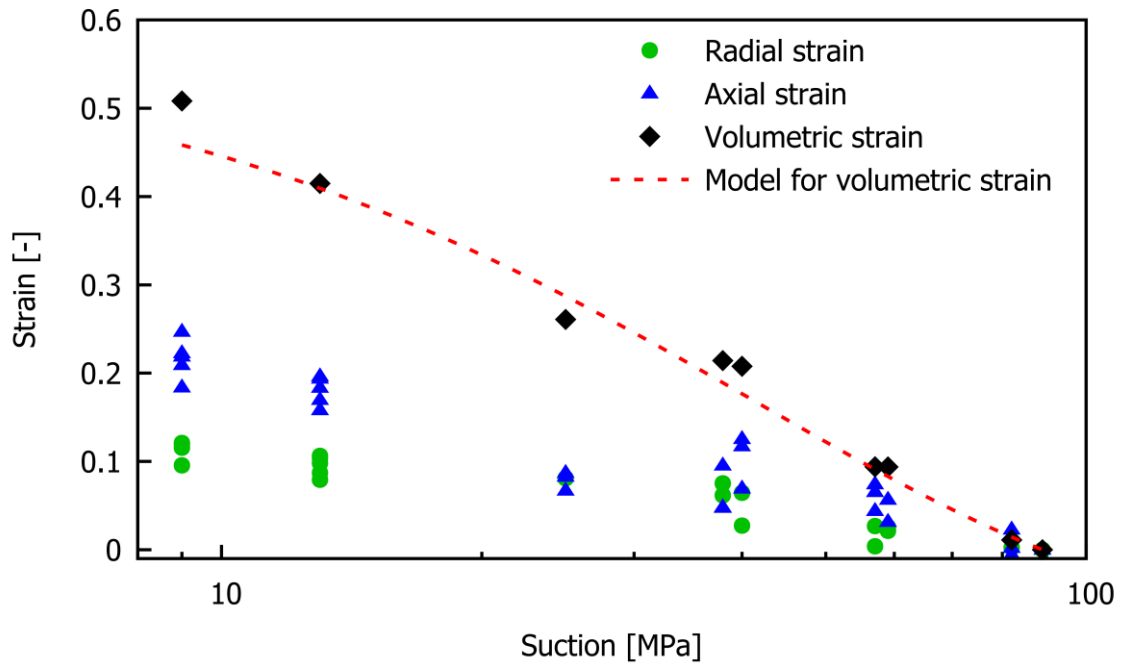


276



277

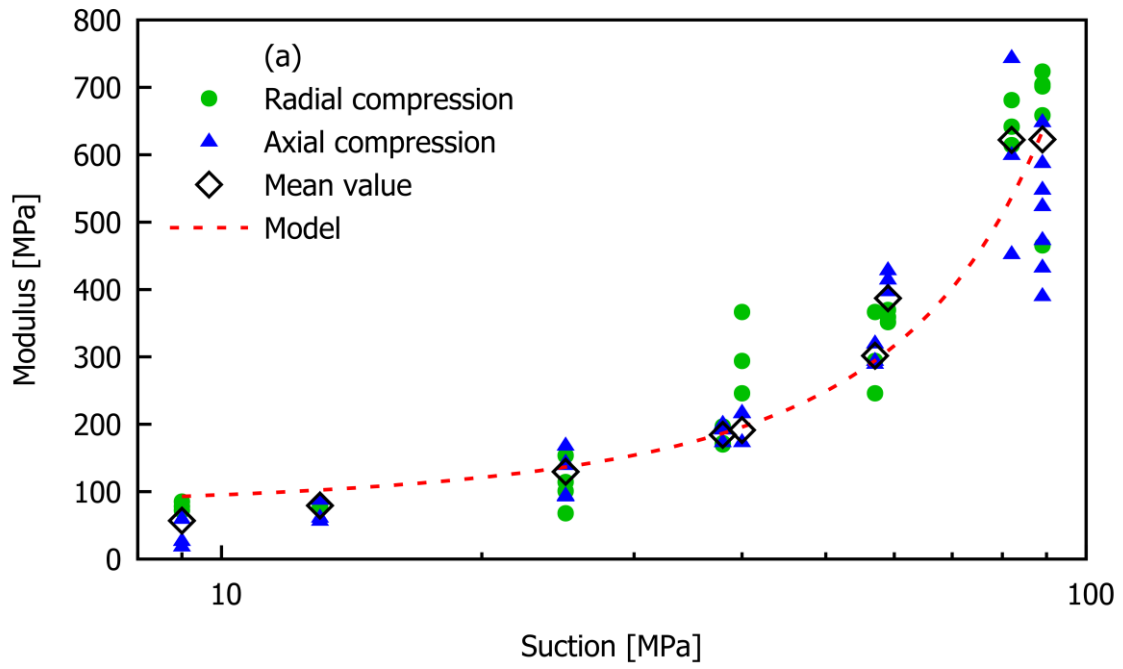
278 Figure 7. Axial, radial and volumetric strains versus suction.



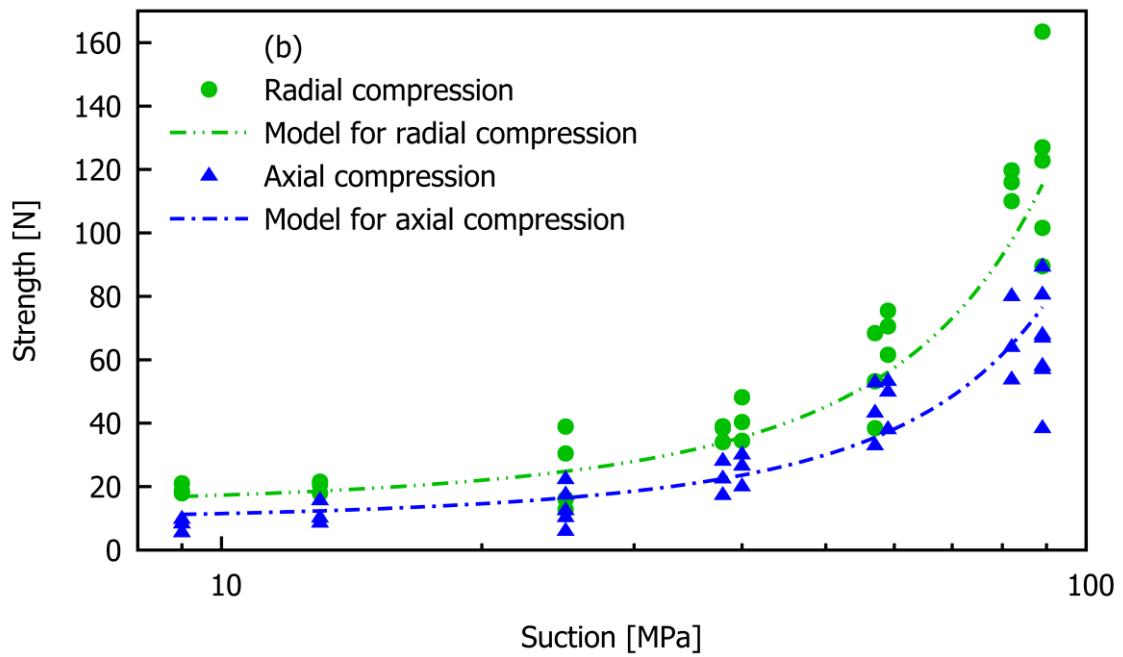
279

280 Figure 8: (a) Modulus versus suction for axial and radial compression tests; (b) Strength versus

281 suction for axial and radial compression tests.

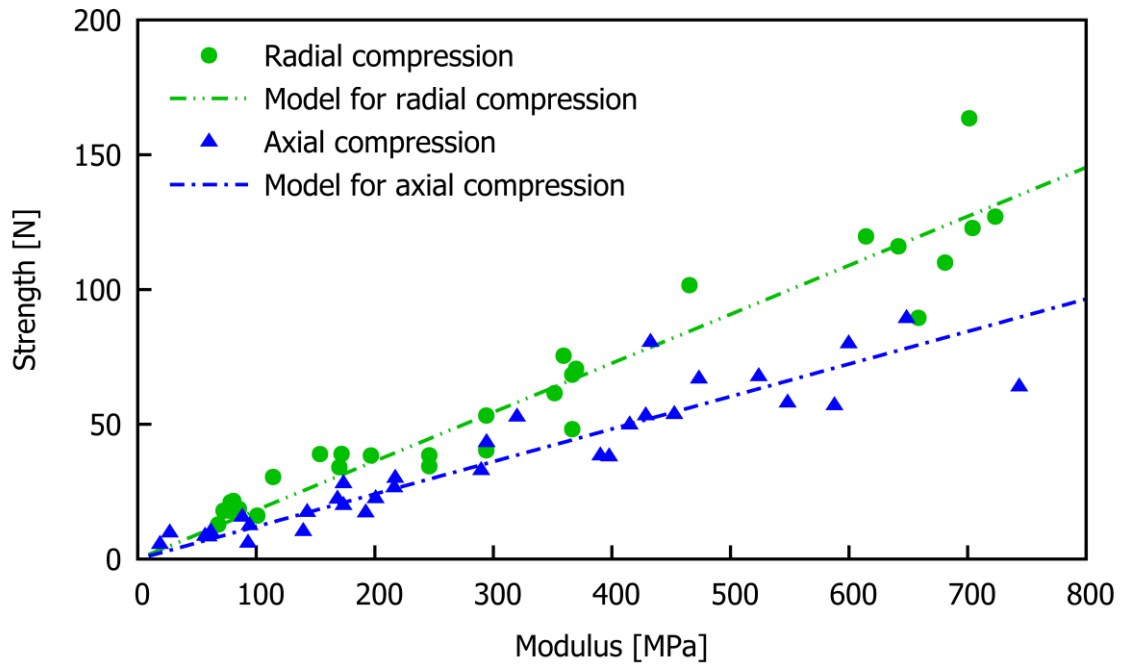


282



283

284 Figure 9: Strength versus modulus for both axial and radial compression tests.



285

286 Table 1. Physical properties of MX80 bentonite

Property	Value
Particle density, $\rho_s$ (Mg/m <sup>3</sup> )	2.77
Smectite content (%)	80
Liquid limit (%)	560
Plastic limit (%)	53
CEC (meq/g)	98/100

287

288 Table 2. Initial properties of the pellets

Property	Value
Dry density, $\rho_d$ (Mg/m <sup>3</sup> )	1.90
Void ratio, $e$ (-)	0.46
Water content, $w$ (%)	12.2
Diameter, $D$ (mm)	7.0
Height, $H$ (mm)	7.0
Height of the cylinder-shaped part, $h$ (mm)	5.0
Curvature radius, $R_c$ (mm)	6.5
Suction, $s_0$ (MPa)	89

289